Progress In Electromagnetics Research, PIER 87, 245–262, 2008

ON THE COMPARISON OF THE SPHERICAL WAVE EXPANSION-TO-PLANE WAVE EXPANSION AND THE SOURCES RECONSTRUCTION METHOD FOR ANTENNA DIAGNOSTICS

Y. Á. López

Area of Signal Theory and Communications
University of Oviedo
Edif. Polivalente, Mod. 8, Campus Universitario de Viesques
E-33203, Gijón, Asturias, Spain

C. Cappellin

TICRA
Læderstræde 34, DK-1201 Copenhagen K, Denmark

F. Las-Heras

Area of Signal Theory and Communications
University of Oviedo
Edif. Polivalente, Mod. 8, Campus Universitario de Viesques
E-33203, Gijón, Asturias, Spain

O. Breinbjerg

Department of Electrical Engineering
Technical University of Denmark
DK-2800 Kgs. Lyngby, Denmark

Abstract—A comparison between two recently developed methods for antenna diagnostics is presented. On one hand, the Spherical Wave Expansion-to-Plane Wave Expansion (SWE-PWE), based on the relationship between spherical and planar wave modes. On the other hand, the Sources Reconstruction Method (SRM), based on the application of the equivalence principle and the integral equations relating fields and sources. In order to compare the results provided by these methods, a reflector antenna has been measured and analyzed.

1. INTRODUCTION

Electrical and mechanical errors in an antenna, due to manufacturing, handling, or aging, may seriously affect the antenna's performance. The presence of such errors is usually detected by anomalies in the far-field pattern but, in most cases, it is not possible to readily identify the errors directly from the pattern anomalies. In consequence, invasive inspection techniques are typically required for the errors identification.

Another method for identifying and quantifying the errors is based on the analysis of the antenna extreme near field; this is referred to as antenna diagnostics. The extreme near-field can be determined from the knowledge of the radiated near- or far-field [1, 8].

The reconstruction of the extreme near-field from near- of far-field measurements has been accomplished through different approaches [5, 7–16]. In particular, a plane-to-plane method for the determination of the aperture field from planar near-field measurements is presented in [7] while [9] describes a method for reflector surface diagnostics from far-field data. In this paper, two recently developed antenna diagnostics methods are compared: On one hand, the Spherical Wave Expansion to Plane Wave Expansion (SWE-PWE), based on the relationship between spherical and planar wave modes [10, 11]; on the other hand, the Sources Reconstruction Method (SRM), which is based on the solution of the integral equations relating fields and currents and the application of the equivalence principle [5, 7, 12–14] (a scalar formulation of the inverse radiation problem is described in [15]).

In order to compare the accuracy and capability of the two diagnostics techniques, an offset reflector antenna with two intentionally introduced surface distortion errors was chosen. This antenna was measured at the DTU-ESA Spherical Near-Field Antenna Test Facility [17], which is operated by the Technical University of Denmark (DTU) for the European Space Agency (ESA).

2. ANTENNA MEASUREMENT SETUP

The Antenna Under Test (AUT) is a commercially available 12 GHz offset parabolic reflector with a circular projected aperture of diameter $D = 60\,\text{cm}$, a focal length $f = 39\,\text{cm}$ and a clearance $d' = 9\,\text{cm}$. The feed is linearly polarized along x_f, where $x_f\, y_f\, z_f$ is the feed Coordinate System (CS), with its origin at the focus and with z_f pointing towards the center point on the reflector, see Fig. 1.

The AUT was mounted on the antenna positioner of the DTU-ESA Facility according to Fig. 2. The measurements CS, $x_{meas}\, y_{meas}\, z_{meas}$,

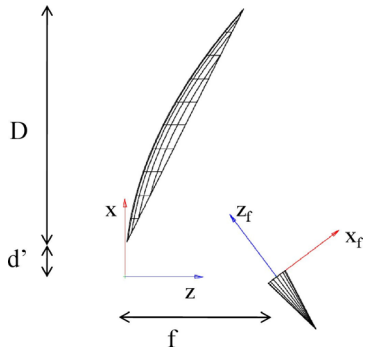

Figure 1. Offset reflector antenna and coordinate systems.

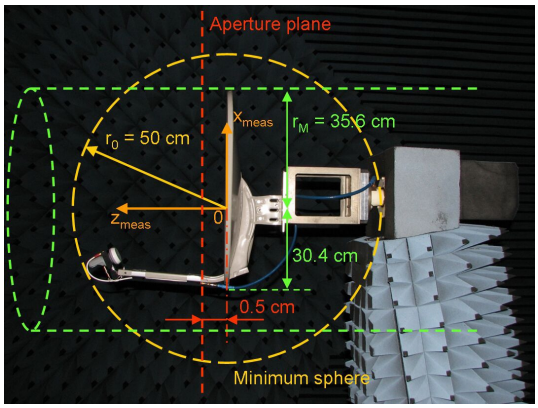

Figure 2. Offset reflector antenna measurement configuration and definition of the aperture plane ($z_{meas} = 0.5\,\text{cm}$) where the field is reconstructed (not to scale).

was defined with origin on the reflector aperture plane and the z_{meas}-axis normal to it and coinciding with the horizontal rotation axis of antenna positioner (Fig. 2) [11].

The radius r_o of the antenna minimum sphere, measured as the distance from the origin of the measurement CS to the feed (see Fig. 2), is equal to $r_o \approx 50\,\text{cm} \approx 20\lambda$, while the radius of the smallest cylinder parallel to the measurement z-axis (z_{meas}) and enclosing the antenna is given by $r_M = 35.6\,\text{cm} = 14\lambda$ (see Fig. 2). This allows us to define the truncation numbers N and M, in the n- and m-modes respectively, to be used in the SWE for an accurate evaluation of the far-field, according to $N = kr_o + 10 = 135$ and $M = kr_M + 10 = 99$ [18],

being k the wavenumber. Though the truncation numbers are obtained from the geometrical dimensions of the AUT in the measurement CS, the n- and m-modes of the SWE are related to each other, being $n = 1, 2, \ldots, N$ and in general $m = -N, -N+1, \ldots, N$. However, since $r_M < r_o$, it is possible to truncate the $m-$modes at M, with $M < N$ and equal to $M = kr_M + 10$, see Fig. 3, while keeping the same accuracy.

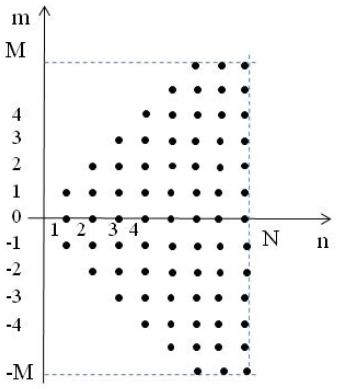

Figure 3. n- and m-modes in the SWE.

With these truncation numbers, a sampling in θ equal to $\Delta\theta = 180^\circ/N \approx 1.33^\circ$, and in φ equal to $\Delta\varphi = 360^\circ/N_\varphi \approx 1.8^\circ$ (with $N_\varphi = 2(M+1)$) was necessary. It was however decided to oversample the radiated field along theta, using $\Delta\theta = 0.5^\circ$ [4]. Due to the antenna size ($r_o = 20\lambda$), the working frequency ($f = 12\,\text{GHz}$) and the separation between the center of the measurement CS and the probe ($6.07\,\text{m} = 242.8\lambda$), measurements were carried out in the antenna near-field region, as the far-field region starts at about $2(2r_o)^2/\lambda = 2592\lambda$.

From the measured near-field and the knowledge of the probe response, the probe-corrected Q coefficients of the spherical wave expansion were calculated and the far-field pattern was determined [3, 4, 18]. From the Q coefficients the power spectrum was then computed (1):

$$\begin{aligned} P_{rad}(n) &= \frac{1}{2}\sum_{m=-n}^{n}\left|Q_{1mn}^{(3)}\right|^2 + \left|Q_{2mn}^{(3)}\right|^2 \\ P_{rad}(|m|) &= \frac{1}{2}\sum_{n=|m|}^{N}\left\{\begin{array}{l}\left|Q_{1mn}^{(3)}\right|^2 + \left|Q_{2mn}^{(3)}\right|^2 \\ +\left|Q_{1-mn}^{(3)}\right|^2 + \left|Q_{2-mn}^{(3)}\right|^2\end{array}\right\} \end{aligned} \tag{1}$$

Figure 4 shows the power spectrum, as determined from Eq. (1), and the truncation numbers $N = 138$ and $M = 70$ obtained because of the finite dynamic range of the measurement system. It is seen that while $N = 138$ is larger than the expected $N = 135 = kr_o + 10$, and thus provides all the necessary modes for a correct evaluation of the far-field, 29 m-modes are missing with respect to the expected $M = 99$. It is possible to see from Fig. 4 that these missing m-modes are however of negligible importance since they have very small amplitude. Moreover, since the AUT is very directive, the information on the radiated field is contained in the first m-modes while the remaining ones mostly express the spillover of the feed and the diffraction from the reflector and the feed arm.

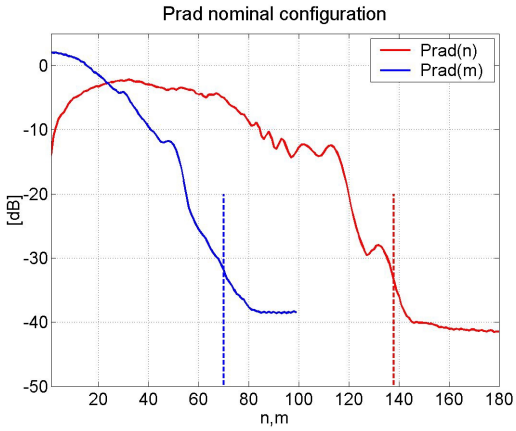

Figure 4. Power spectrum in the measurement CS of the antenna and the truncation numbers $N = 138$, $M = 70$.

The Q coefficients determined from the near-field measurement and the obtained far-field were used as input to the SWE-PWE and SRM algorithms, respectively, in order to compute the extreme near-field on the reference aperture plane ($z_{meas} = 0.5\,\mathrm{cm}$).

2.1. Spherical Wave Expansion-Plane Wave Expansion

From the Q coefficients of the SWE, the plane wave spectrum at any given coordinate z, $\bar{T}(k_x, k_y, z) = \bar{T}(k_x, k_y)e^{jk_z z}$ in the spectral $k_x k_y$-domain is first computed according to (2):

$$\bar{T}(k_x, k_y, z) = \sum_{n=1}^{\infty} \sum_{m=-n}^{n} \left\{ \begin{array}{l} Q_{1mn}^{(3)} \bar{T}_{1mn}(k_x, k_y, z) + \\ Q_{2mn}^{(3)} \bar{T}_{2mn}(k_x, k_y, z) \end{array} \right\} \qquad (2)$$

Details about the functions $\bar{T}_{1mn}(k_x, k_y, z), \bar{T}_{2mn}(k_x, k_y, z)$ and spectral variables used can be found in [10] or [11]. Here it is only recalled that the spectral $k_x k_y$-domain is divided into two regions, according to the relationship between the Cartesian components of the wave propagation vector $\bar{k} = k_x\hat{x} + k_y\hat{y} + k_z\hat{z}$: $k_z = (k^2 - k_x^2 - k_y^2)^{1/2}$. The visible region corresponds to $k_x^2 + k_y^2 \leq k^2$, with $k = 2\pi/\lambda$ being the wave number, which contains the propagating plane waves, and the invisible region, for $k_x^2 + k_y^2 > k^2$, which contains the evanescent plane waves.

Eq. (2) allows one to compute the plane wave spectrum from the Q coefficients in the visible region and, in principle, also in the invisible region. In practice, the finite dynamic range of the system truncates the n- and m-modes of the spherical wave expansion, limiting the spectral region in which the spectrum computed by Eq. (2) reaches convergence. In the present case, with the truncation modes $N = 138$ and $M = 70$ shown in Fig. 4, only the visible part of the plane wave spectrum and the singularity at $k_z = 0$, i.e., at the border between the visible and invisible region, can be recovered.

Once the plane wave spectrum is known, the aperture field on a z-plane in the source-free region of the AUT is obtained by an inverse Fourier transform (3),

$$\bar{E}(x, y, z) = \frac{1}{2\pi} \int_{-\infty}^{\infty} \int_{-\infty}^{\infty} \bar{T}(k_x, k_y) e^{ik_z z} e^{i(k_x x + k_y y)} dk_x dk_y \qquad (3)$$

which is properly modified in order to extract the spectral singularity that can exist at the border $k_z = 0$. It is noted that in the present case the plane $z_{meas} = 0.5\,\text{cm}$ on which the field is reconstructed is not in the source free-region of the antenna, since the plane is located behind the feed. This can however be accepted since the main contribution to the measured field is given by the radiation from the reflector, while the field from the feed is directed towards the reflector and should in principle be shadowed by it. On the other hand it is true that the measured field contains also information on the effect of the feed in the far-field and the scattering both from the feed arm and the edge of the reflector dish. Thus, the field computed by Eq. (3) on the plane $z_{meas} = 0.5\,\text{cm}$ is in this case not the pure field radiated by the main reflector, but it represents all the effects which are present over the measurement surface.

2.2. Sources Reconstruction Method

The Sources Reconstruction Method (SRM) is based on the determination of a set of equivalent electric and magnetic currents that radiate the same field outside the original sources domain (Electromagnetic Equivalence Principle) [7, 8, 12, 13]. In the case of aperture antennas, it is possible to apply the Image Theory in order to simplify the problem, so that the original sources are characterized through an equivalent magnetic currents distribution on the aperture plane (S_{ap}), which are related to the tangential electric field on this plane (see Fig. 5).

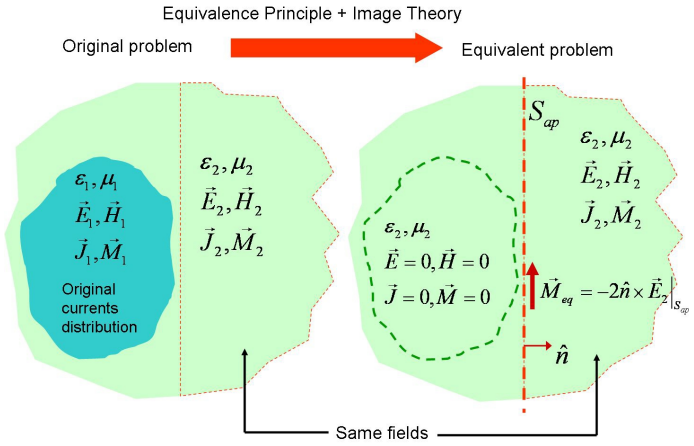

Figure 5. Equivalence principle and image theory.

The equivalent magnetic currents on the aperture plane are calculated from the radiated field (NF or FF) by solving the integral equation (4):

$$\bar{E}(\bar{r}) = -\frac{1}{4\pi}\nabla \times \int_{S_{ap}} \bar{M}_{eq}(\bar{r}') \frac{e^{-jkR(\bar{r};\bar{r}')}}{R(\bar{r};\bar{r}')} dS_{ap} \tag{4}$$

where $R(\bar{r};\bar{r}') = |\bar{r} - \bar{r}'|$, with $\bar{r} = \bar{r}(x, y, z)$ being the position vector for observation points and $\bar{r}' = \bar{r}'(x', y', z')$ the position vector for the sources.

From a theoretical point of view, the aperture plane should be infinite. However, it is possible to truncate it as the radiated power of the antenna, and thus the equivalent currents, is concentrated in a finite region. Thus, the plane size has been limited to an 80×80 cm

domain. Regarding the equivalent currents domain discretization, a mesh with values $\Delta x_{meas} = \Delta y_{meas} = 0.25\lambda$ has been used on the aperture plane ($z_{meas} = 0.5\,\text{cm}$) while for the required FF sampling rate, the SWE sampling rule described above and in [18] was considered, providing $\theta = [0°, -180°]$ being the θ-step ($\Delta\theta$) equal to 1°, and $\varphi = [0°, -360°]$ being the φ-step ($\Delta\varphi$) equal to 1°. The application of the Image Theory requires to consider the field only in the front half space ($z_{meas} > 0$): $\theta = [0°, -90°]$.

Concerning the SRM computational cost, the number of Conjugate Gradient (CG) [19, 20] iterations for solving the system of equations [14] was set to 15. A larger number of iterations increase the computational cost, and the Root Mean Square Error (RMSE) has not a significant additional decrease. Regarding the numerical solution, the number of equations was 36,400 and the number of unknowns 32,768 [14].

3. RESULTS

The following section shows the reflector antenna diagnostics results for two cases in which the reflector is distorted from its nominal configuration. In the first case, a metallic bump is attached to the reflector dish. In the second case, 21 dishes are placed arbitrarily over the reflector surface.

3.1. Gaussian Bump Attached to the Reflector Surface

A metallic bump with the shape of a two-dimensional Gaussian function (peak and standard deviation are both 1 cm) was built and attached to the reflector surface, as shown in Fig. 6. From the measured Q coefficients and the transformed FF, the electric field and the equivalent magnetic currents were calculated on the aperture plane

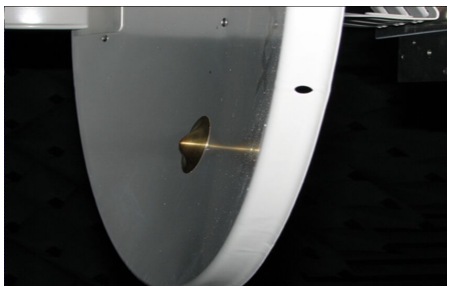

Figure 6. Gaussian bump on the reflector surface.

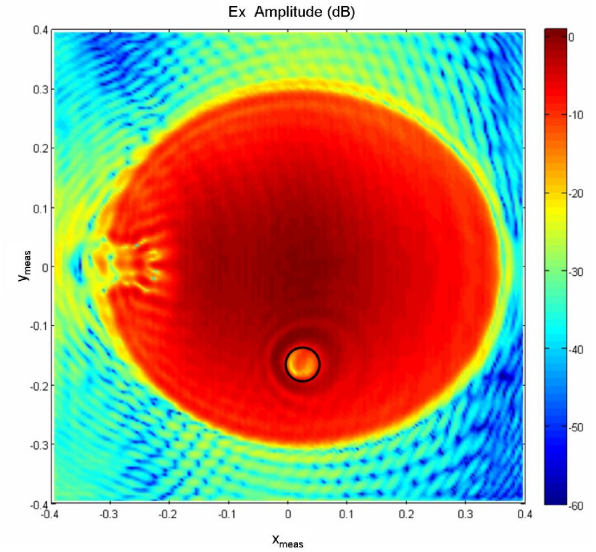

(a)

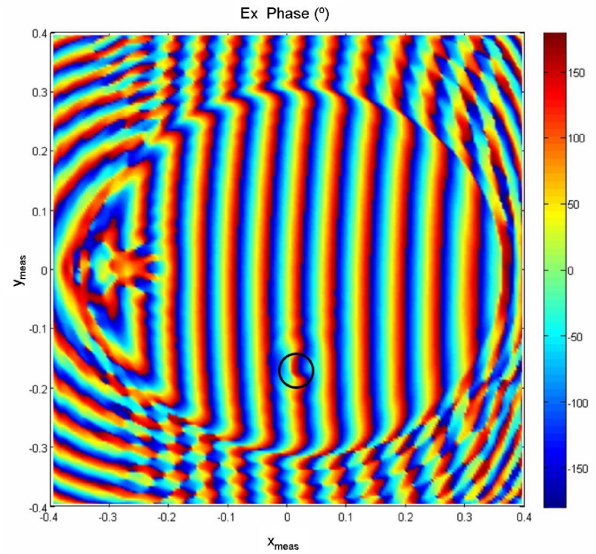

(b)

Figure 7. (a) Amplitude and (b) phase of the E_x reconstructed on the aperture plane ($z_{meas} = 0.5\,\text{cm}$) using the SRM.

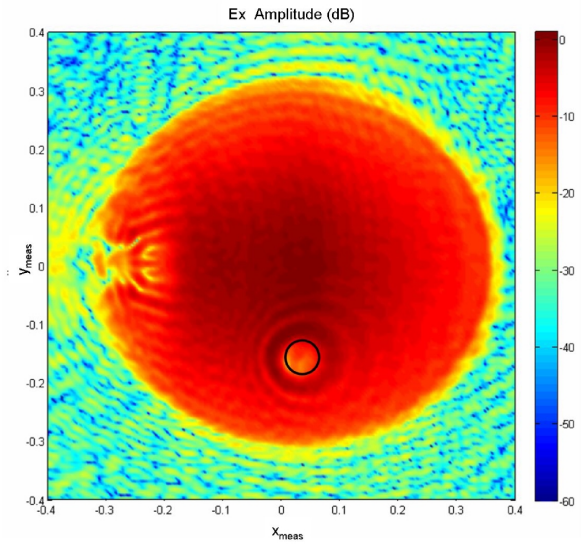

(a)

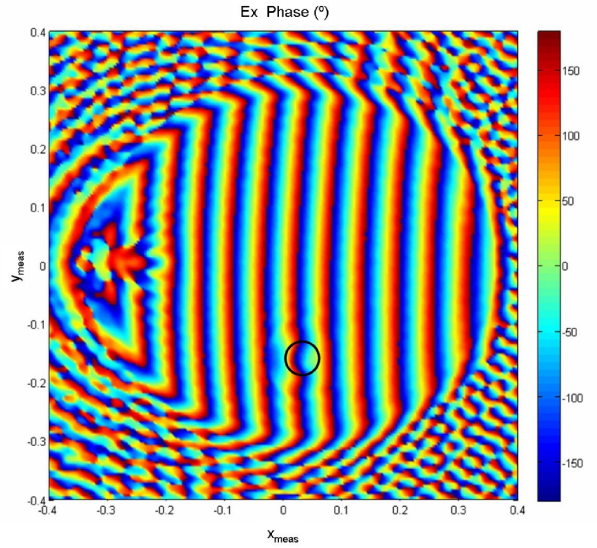

(b)

Figure 8. (a) Amplitude and (b) phase of the E_x reconstructed on the aperture plane ($z_{meas} = 0.5\,\text{cm}$) using the SWE-PWE.

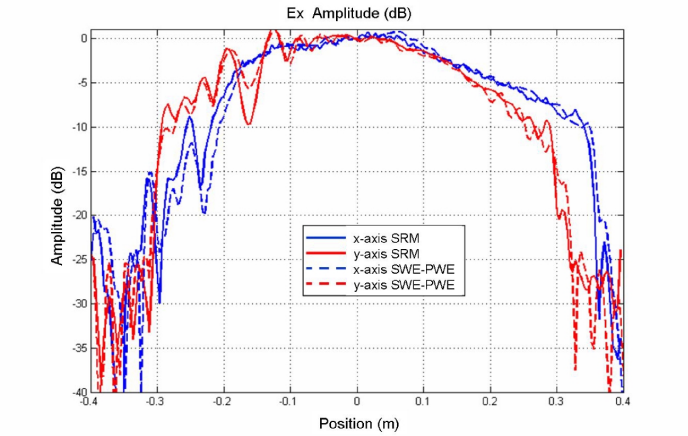

(a)

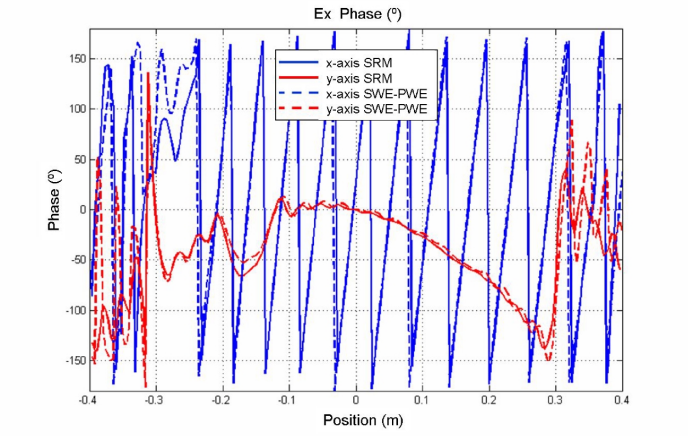

(b)

Figure 9. Comparison between E_x calculated using the SRM and the SWE-PWE techniques along the x_{meas}- and y_{meas}-axes on the aperture plane: (a) amplitude, (b) phase.

with the SWE-PWE and SRM techniques respectively. The Gaussian bump is clearly identified by the SRM in Fig. 7 and by the SWE-PWE in Fig. 8, both in amplitude and phase.

Figure 9 shows the x-component of the electric field along the x_{meas}- and y_{meas}-axes on the aperture plane ($z_{meas} = 0.5\,\text{cm}$) for the two compared techniques. The results show a good agreement with differences below 1 dB in amplitude, and ± 10 deg. in phase, in

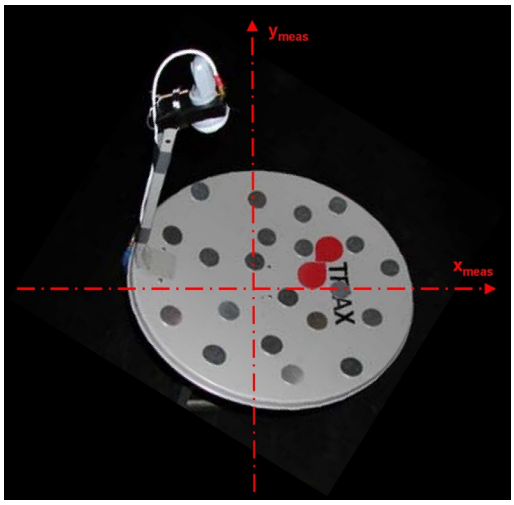

Figure 10. Antenna with the aluminum dishes.

the aperture plane corresponding to the reflector projection where the illumination is uniform. These differences increase for lower field levels corresponding to the area outside the projected aperture, as well as over the bump and close to the connection of the feed arm with the reflector. It is important to notice that the phase distortion (≈ 60 deg.) due to the bump which is clearly seen in the "y"-axis gives a good estimation of the bump height: 83 mm.

3.2. Surface Distortion with 21 Aluminum Dishes

The reflector antenna surface was then distorted by randomly placing 21 dishes of aluminum with diameter of 5 cm and thicknesses of 2.5 mm, 1.5 mm and 1 mm ($\lambda = 2.5$ cm) on the entire reflector surface (see Fig. 10).

Figure 11 shows the amplitude and the phase of the x-component of the electric field calculated using the SRM method, while the same field component reconstructed using the SWE-PWE is plotted in Fig. 12. In both figures, the estimated position of the aluminum dishes is remarked with black circles. These positions have been compared with a picture of the antenna with the dishes (Fig. 10), showing a good agreement between the estimated positions and the original ones. The amplitude and phase of E_x along the x_{meas} and y_{meas} axes on the aperture plane ($z_{meas} = 0.5$ cm) obtained by SRM are compared with the reconstructed field using the SWE-PWE in Fig. 13.

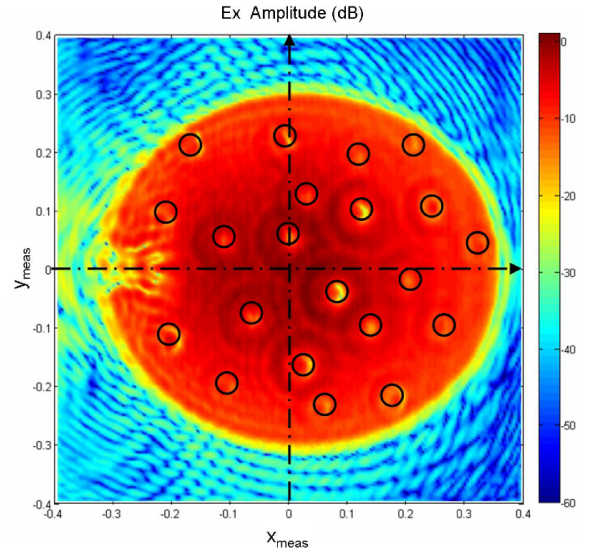

(a)

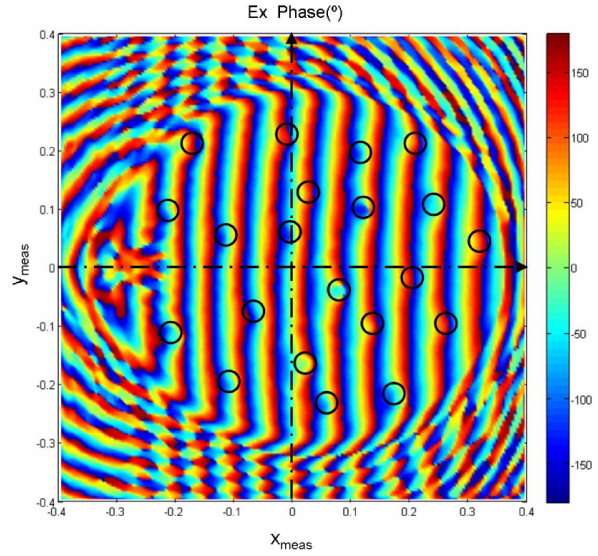

(b)

Figure 11. (a) Amplitude and (b) phase of the E_x reconstructed on the aperture plane ($z_{meas} = 0.5\,\text{cm}$) using the SRM.

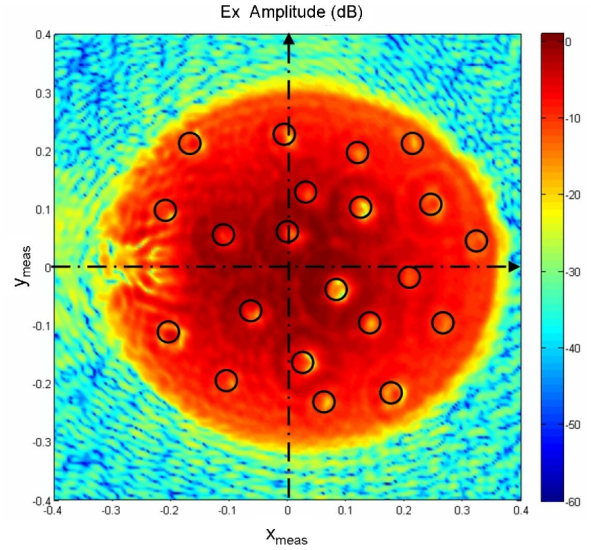

(a)

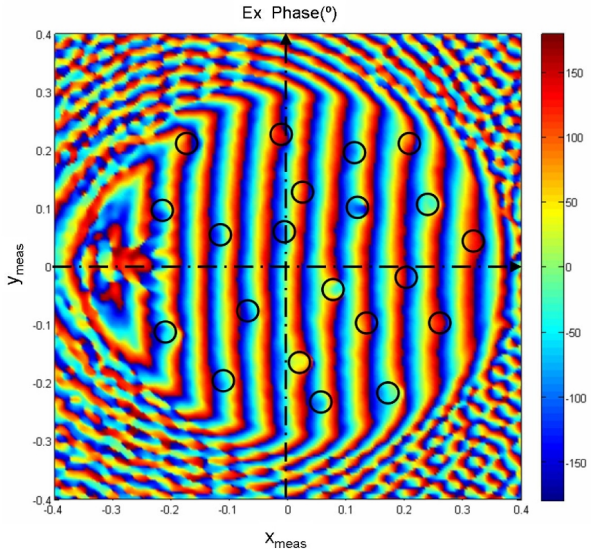

(b)

Figure 12. (a) Amplitude and (b) phase of the E_x reconstructed on the aperture plane ($z_{meas} = 0.5\,\text{cm}$) using the SWE-PWE.

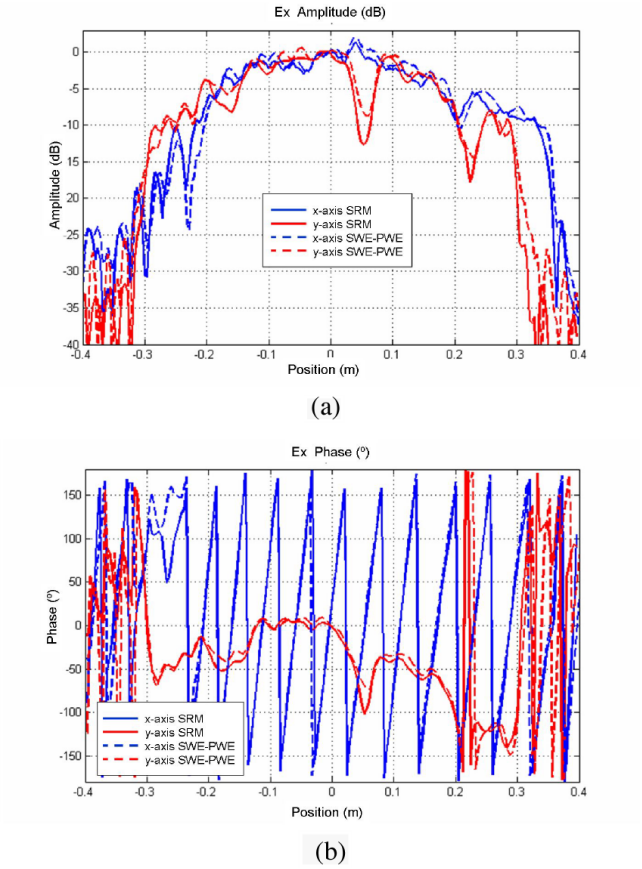

Figure 13. Comparison between E_x calculated using the SRM and the SWE-PWE techniques along the x_{meas}- and y_{meas}-axes on the aperture plane: (a) amplitude, (b) phase.

4. CONCLUSIONS

Two antenna diagnostics methods have been compared: the SWE-PWE method, which is based on the relationship between spherical and planar wave modes, and the SRM, founded on the application of the equivalence principle and the integral equations relating fields and sources.

The different theoretical foundations are related to the field of application of each method. The SWE-PWE allows the diagnostics of antennas through the analysis of the field in the aperture plane. This includes, for example, the detection of malfunctioning elements

in antenna arrays, or the detection of surface anomalies in reflector antennas. The SRM extends the SWE-PWE capabilities allowing the calculation of the extreme near field over arbitrary surfaces, and can thus be used in analyzing for example radome-covered antennas.

Despite the different foundations and fields of application of these two antenna diagnostics methods, there are some cases in which both methods can be applied in the same way, e.g. the example shown in this paper: two different reflector antenna configurations were analyzed, being the goal the detection of reflector surface distortions.

From the results it can be concluded that the SWE-PWE and the SRM yield almost the same and accurate results, being the differences between them less than 1 dB in amplitude and less than 10° in phase in the projected reflector antenna aperture area (where the field amplitude has the maximum value and is mostly uniform).

Regarding the location of the anomalies, for the two proposed configurations, both methods are able to determine the metallic bump and aluminum dishes respectively. Differences between the reconstructed fields increase until 5 dB in amplitude and 20° in phase over the area where the anomalies are placed. These discrepancies between the reconstructed fields can be explained by the different theoretical foundations of the methods. More in detail, the SWE-PWE requires a field acquisition over the entire spherical domain and allows the determination of the three field components (E_x, E_y, E_z) on the zmeas = 0.5 cm plane whereas the SRM, with the application of the Image Theory, works with the field only in the hemisphere $z_{meas} > 0$ and retrieves the tangential components E_x, E_y.

ACKNOWLEDGMENT

This work has been supported by COST IC0603 ("ASSIST") action through a Short Term Scientific Mission grant. Also, by the "Ministerio de Ciencia e Innovación" of Spain /FEDER" under projects TEC2008-01638/TEC (INVEMTA) and CONSOLIDER CSD2008-00068 (TERASENSE), and by the "Cátedra Telefónica- Universidad de Oviedo".

REFERENCES

1. Ponnapalli, S., "Near-field to far-field transformation utilizing the conjugate gradient method," *Progress In Electromagnetics Research*, PIER 05, 391–422, 1991.
2. Costanzo, S. and G. Di Massa, "Far-field reconstruction from phaseless near-field data on a cylindrical helix," *Journal of*

Electromagnetic Waves and Applications, Vol. 18, No. 8, 1057–1071, 2004.

3. Koivisto, P., "Reduction of errors in antenna radiation patterns using optimally truncated spherical wave expansion," *Progress In Electromagnetics Research*, PIER 47, 313–333, 2004.
4. Koivisto, P. and J. C.-E. Sten, "On the influence of incomplete radiation pattern data on the accuracy of a spherical wave expansion," *Progress In Electromagnetics Research*, PIER 52, 185–204, 2005.
5. Ayestarán, R. G. and F. Las Heras, "Near field to far field transformation using neural networks and source reconstruction," *Journal of Electromagnetic Waves and Applications*, Vol. 20, 2201–2213, 2006.
6. Costanzo, S. and G. DiMassa, "Near-field to far-field transformation with planar spiral scanning," *Progress In Electromagnetics Research*, PIER 73, 49–59, 2007.
7. Petre, P. and T. K. Sarkar, "Planar near-field to far-field transformation using an equivalent magnetic current approach," *IEEE Transactions on Antennas and Propagation*, Vol. 40, No. 11, 1348–1356, Nov. 1992.
8. Sarkar, T. K., P. Petre, A. Taaghol, and R. F. Harrington, "An alternative spherical near field to far field transformation," *Progress In Electromagnetics Research*, PIER 16, 269–284, 1997.
9. Rahmat-Samii, Y., "Surface diagnosis of large reflector antennas using microwave holographic metrology: An iterative approach," *Radio Science*, Vol. 19, 1205–1217, 1984.
10. Cappellin, C., O. Breinbjerg, and A. Frandsen, "Properties of the transformation from the spherical wave expansion to the plane wave expansion," *Radio Science*, Vol. 43, RS1012, 2008.
11. Cappellin, C., A. Frandsen, and O. Breinbjerg, "Application of the SWE-to-PWE antenna diagnostics technique to an offset reflector antenna," *AMTA 2007 Symposium*, St. Louis, USA, 2007. Available at: http://support.ticra.com/public/A07-0056.pdf Also to be published in *IEEE Antennas and Propagation Magazine*, Dec. 2008.
12. Petre, P. and T. K. Sarkar, "Differences between modal expansion and intergral equation methods for planar near-field to far-field transformation," *Progress In Electromagnetics Research*, PIER 12, 37–56, 1996.
13. Las-Heras, F., M. R. Pino, S. Loredo, Y. Alvarez, and T. K. Sarkar, "Evaluating near field radiation patterns of

commercial antennas," *IEEE Transactions on Antennas and Propagation*, Vol. 54, No. 8, 2198–2207, Aug. 2006.

14. Alvarez, Y., F. Las-Heras, and M. R. Pino, "Reconstruction of equivalent currents distribution over arbitrary three-dimensional surfaces based on integral equation algorithms," *IEEE Transactions on Antennas and Propagation*, Vol. 55, No. 12, 3460–3468, Dec. 2007.
15. Persson, K. and M. Gustafson, "Reconstruction of equivalent currents using a near-field data transformation — with radome application," *Progress In Electromagnetics Research*, PIER 54, 179–198, 2005.
16. Kaplan, L., J. D. Hanfling, and G. V. Borgiotti, "The backward transform of the near field for reconstruction of aperture field," *IEEE Antennas and Propagation Society Symposium Dig.*, 764–767, 1979.
17. Homepage of the DTU-ESA Facility: http://www.oersted.dtu.dk/English/research/emi/afg/dtu_esa_facility.aspx.
18. Hansen, J. E., *Spherical Near-Field Antenna Measurements*, Peter Peregrinus Ltd., London, 1988.
19. Roger, A. and F. Chapel, "Iterative methods for inverse problems," *Progress In Electromagnetics Research*, PIER 05, 423–454, 1991.
20. Carpentieri, B., "Fast iterative solution methods in electromagnetic scattering," *Progress In Electromagnetics Research*, PIER 79, 151–178, 2008.